An investigation of the solar irradiance effect on visible light communications

An Investigation of the Sunlight Irradiance Effect on Visible Light Communications

Mohamed Sufyan Islim and Harald Haas

LiFi Research and Development Centre, Institute for Digital Communications
University of Edinburgh, King's Buildings, Mayfield Road, Edinburgh, EH9 3JL, UK
Email: {m.islim, h.haas}@ed.ac.uk

***Abstract*—This work aims to debunk the myth that visible light communication (VLC) systems can not work under the presence of sunlight. It provides an investigation of an outdoor VLC system model in the presence of sunlight irradiance. Worst-case scenarios are considered in terms of location, link orientation and choice of photodiode. The effect of sunlight irradiance is investigated in terms of data rate and bit error rate (BER) degradation. An optical bandpass blue filter is shown to compensate for half of the reduced data rate in the presence of sunlight. Reliable communications in the order of hundreds of Mb/s can be achieved using simple optical filtering under the effect of sunlight irradiance.**

I. Introduction

Traffic from wireless and mobile devices will account for two-thirds of the total internet traffic by 2020 [1]. The radio frequency (RF) bandwidth is a scarce resource costing above £1m ($1.28m) per 1 MHz in the 2.4 GHz frequency band in the UK [2]. Visible light communication (VLC) offers a much larger frequency bandwidth that is unlicensed and safe to use. The VLC has the potential to reuse the existing lightning infrastructure for communications purposes [3]. Light fidelity (LiFi) is the network solution for VLC that is supposed to work seamlessly beside other RF access technologies [3]. A record data rate of 7.91 Gb/s was reported for orthogonal frequency division multiplexing (OFDM)-based VLCs using single violet micro-scale GaN light emitting diode (LED) (m-LED) [4]. Data rates above 100 Gb/s can be achived if the complete visible spectrum is utilized [5].

The effect of sunlight irradiance on VLC is considered to be one of the main misconceptions surronding VLC [6]. It is generally assumed that it could halt the operation of the communication system entirely due to the interference. However, the effect of sunlight irradiance is more apparent as a strong shot noise source rather than an interferernce source as the sunlight intensity does not vary tremendously over short periods of time. This allow multicarrier schemes such as OFDM to allocate the symbols over the usable frequency subcarriers of the deployed bandwidth [7].

The effect of sunlight irradiance on the performance of optical wireless communications (OWC) and VLC has been invistigated in the published research [8]–[10]. The use of optical filters with a special layer of microlouver to mitigate the effect of sunlight was suggested in [8]. However, the microlouver layer restricts the field of view (FOV) of the photodetector, which limits the overall system to narrow FOV communications. The performance of VLC systems in the presence of sunlight irradiance was studied using computer simulations in [9]. The sunlight irradiance was assumed to be incident from a window and reflected on multiple walls before it is collected by the photodiode. The performance degradation was estimated using the theoretical model for the incident sunlight irradiance in two geographic locations. However, the performance of an outdoor VLC system was not considered. The impact of sunlight irradiance on the performance of underwater OWC links was investigated for positive-intrinsic-negative (PIN) and avalanche photodiode (APD) in [10], where it was shown that sunlight affects the system performance at relatively low depths.

In this paper, we investigate the performance of outdoor VLC systems under sunlight irradiance. Worst-case scenarios are considered in terms of time and location. The investigation compares the use of a bandpass optical blue filter to the case where a filter is not considered in front of the photodetector. The performance is compared to a benchmark scenario of a dark room where sunlight does not reach the photodetector. The performance comparison is based on the predicted solar irradiance. The results show the sunlight irradiance to be affecting, but not significantly degrading, the performance of VLC. In addition, it is shown that 50% of the losses in data rate performance can be recovered using an inexpensive commercially available bandpass blue filter.

The rest of this paper is organized as follows. In Section II, we review an algorithm to calculate the position and irradiance of the sun at any given location and time. The assumptions of this investigation are specified in Section III-A. The signal-to-noise ratio (SNR), maximum achievable data rate and bit error rate (BER) of the system are derived and the system modelling is discussed in Section III-B. The system performance is analyzed and the results are shown in Section IV. Section V concludes the paper.

II. Solar Irradiance and Position

The solar constant flux density P_{SC} is given as 1366.1 w/m^2 outside the Earth atmosphere by the American society for testing and materials (ASTM) standard (ASTM E-490) [11]. The sunlight irradiance is not limited to the visible spectrum as it spans the wavelengths from 250 nm to 2500 nm. The solar irradiance at different wavelengths is non-equally attenuated as it travels through the atmosphere due to the different

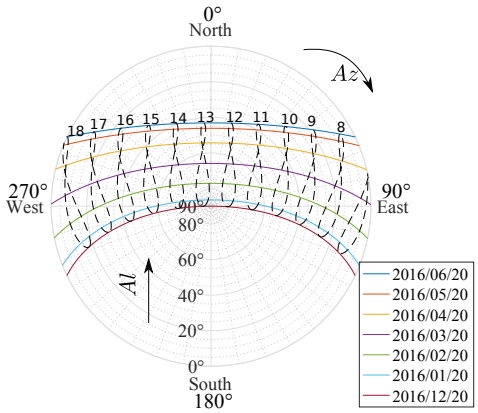

Fig. 1. Solar position described by altitude and azimuth for Antofagasta, Chile on the 20th of each considered month. The time of the day is listed above the elliptical shapes which represents the analemma diagrams.

absorption and scattering effects of the air molecules and aerosols of the atmosphere. The shortest path for the sunlight exists when the Sun is located at the zenith point (imaginary point above the head of the observer). The optical air mass (AM) is approximated as the ratio of the actual sunlight path to the minimum path at zenith point. It is given as AM0 for the extraterrestrial irradiance. When the Sun is at angle θ_Z relative to the zenith, the optical AM is approximated as:

$$\mathrm{AM} \simeq \frac{1}{\cos\theta_\mathrm{Z}}. \tag{1}$$

The solar irradiance at $\theta_Z = 48.2°$ is given at an AM1.5 by the standard (ASTM E-490) [12] as a reference to help the solar energy community in testing and comparing the performance of various solar cells. However, the solar irradiance varies based on the geographical location; seasonal and diurnal variations arising from the rotation of the Earth around the Sun; and the rotation around its own axis. The effect of sunlight irradiance on VLC varies based on the time and location. Therefore, it is essential to calculate the position of the Sun in the sky in order for the solar irradiance at particular time and position to be estimated. Various algorithms with different complexities and accuracies for calculating the solar position exists in the astrophysics literature [13]. In this section, we review a simple algorithm based on the ecliptic coordinates with an accuracy of (1/60)° presented in [14] and proposed by the astronomical applications department of the U.S. naval observatory [15].

The horizontal coordinate system is usually used for solar energy applications where the horizon of the observer is considered to be the fundamental plane. The solar position can be described using two angles: altitude Al, and azimuth Az. The solar altitude $Al \in [0°, 90°]$ is given as the elevation of the Sun above the horizon. A solar altitude of $Al = 90°$ means that the Sun is at the zenith point. The solar altitude can also be given as θ_Z as $Al = 90° - \theta_Z$. The solar azimuth $Az \in [0°, 360°]$ is given as the angle between the north and the horizontal projection of the line-of-sight (LoS) between the Sun and the observer. Both angles are illustrated in Fig. 1 for Antofagasta, Chile on the 20th of each considered month. The solar altitude is shown to reach the zenith $Al = 90°$ around 13:00 on the 20th of December 2016. The time of the day is shown above the analemma diagrams which represent the shape of the Sun motion throughout the year when observed on the same hour of the day and at the same location. The solar position, based on the horizontal coordinates, can be calculated using [14]:

$$\sin Al = \cos\phi_0 \cos\theta_L \cos\lambda_\mathrm{S} + (\cos\phi_0 \sin\theta_L \cos\epsilon + \sin\phi_0 \sin\epsilon) \sin\lambda_\mathrm{S} \tag{2}$$

$$\tan Az = \frac{\Gamma_1}{\Gamma_2 - \Gamma_3}, \tag{3}$$

where:

$$\Gamma_1 = -\sin\theta_L \cos\lambda_\mathrm{S} + \cos\theta_L \cos\epsilon \sin\lambda_\mathrm{S}, \tag{4}$$

$$\Gamma_2 = -\sin\phi_0 \cos\theta_L \cos\lambda_\mathrm{S}, \tag{5}$$

$$\Gamma_3 = \sin\lambda_\mathrm{S}(\sin\phi_0 \sin\theta_L \cos\epsilon - \cos\phi_0 \sin\epsilon), \tag{6}$$

where ϕ_0 is the local latitude of the observer. The axial tilt between the equatorial plane and the ecliptic plane ϵ is given as [14]:

$$\epsilon = 23.429° - 0.00000036°D. \tag{7}$$

where D is the time elapsed since the Greenwich noon of the 1st of January 2000. The axial tilt is zero valued in March/September equinox (20th March/September 2016) and takes a maximum value of around $\pm 23.429°$ in June/December solstice (20th June/December 2016). The local mean sidereal time (LMST) θ_L is the angle between March equinox and the meridian (an imaginary circle given at longitude of 0° and passing through the north and south poles and the zenith of an observer). A sidereal day is the time required for the Earth to complete a 360° rotation on its own axis. It is slightly shorter than the solar day mainly due to the rotation of the Earth around the Sun. The LMST can be given as:

$$\theta_L = \mathrm{GMST}\frac{15°}{\mathrm{hour}} + \lambda_0, \tag{8}$$

where λ_0 is the longitude of the observer, and GMST is the Greenwich mean sidereal time (GMST), which can be defined as the hour angle between the March equinox and the meridian at Greenwich. GMST is calculated as:

$$\mathrm{GMST} = 18.697374558\mathrm{h} + 24.06570982441908D, \tag{9}$$

where it is scaled to values $\mathrm{GMST} \in [0, 24]$. The ecliptic longitude λ_S is given as [14]:

$$\lambda_\mathrm{S} = q + 1.915° \sin g + 0.020° \sin 2g, \tag{10}$$

where q is the mean longitude given as [15]:

$$q = 280.459° + 0.98564736°D, \tag{11}$$

and g is the mean anomaly of the Sun which accounts for the varying speeds of the Earth motion throughout the year. This is given as [15]:

$$g = 357.529° + 0.98560028°D, \tag{12}$$

TABLE I
MODELLING ASSUMPTIONS

Location	Antofagasta, Ch 23° 27'16.1"S 70°26'21.4"W
Dates	20th June/December 2016
APD model	Hamamatsu S8664-50K
APD detection area, A	19.6 mm^2
Bandwidth, B	60 MHZ
APD gain, M	100
Dark current, $I_{\rm d}$	3 nA
Blue filter FWHM	50 nm
Received optical power, $P_{\rm R}^{\rm L}$	2.5 mW

Direct sunlight irradiance is the sunlight that is directly reaching the surface of the Earth. Global solar irradiance is the combination of the direct and diffused sunlight irradiance. The direct sunlight irradiance can be calculated using the simple model of the atmospheric radiative transfer of sunshine (SMARTS) which is a parametrized transmittance model to evaluate the solar irradiance at any particular time and location [16], [17] under different atmospheric conditions. The model is used in generating the ASTM standard (ASTM E-490) with a resolution of 0.5-1 nm [11] .

III. Theoretical Study

A. Assumptions

An OFDM-based VLC system is assumed due to its robustness against background illumination flickering. A real-valued OFDM waveform with a direct current (DC) bias is used to modulated the intensity of the LED in what is known as DC-biased optical OFDM (DCO-OFDM). Binary inputs are encoded into multiple M-ary quadrature amplitude modulation (M-QAM) symbols which are allocated into $N_{\rm FFT}$ subcarriers over a single-sided bandwidth of B. Three scenarios are considered:

- *Dark room (Scenario I)*: assumes an optimal case where no background illumination is reaching the photoreceiver.
- *with blue filter (Scenario II)*: assumes that the sunlight irradiance is collected with a bandpass blue filter in front of the photoreceiver.
- *w/o blue filter (Scenario III)*: assumes that the sunlight irradiance is collected without any optical filtering in front of the photoreceiver.

The system assumes a blue m-LED with a pixel size of 100 μm $\times$ 100 μm and a focusing aspheric condenser optical lens (Thorlabs, ACL4532U-A). An optical bandpass blue filter from Edmund Optics is assumed in Scenario II with a centre wavelength of 450 nm, a transmittance higher than 90%, and a full width at half maximum (FWHM) of 50 nm. The photoreceiver is an APD (Hamamatsu, S8664-50K) where it is always assumed to be aligned with the m-LED. A choice of other types of photoreceivers is possible. However, APDs are used as a worst case choice in this investigation as they are shot-noise limited [18]. The APD will not be always collecting the sunlight irradiance due to the orientation of the communications link in practical situations. However, the APD is always assumed to be collecting the sunlight in this investigation.

The location considered is 23°27'16.1"S 70°26'21.4"W in Antofagasta, Chile which is claimed to have the highest solar radiation on Earth [19]. The model considers two dates: summer solstice and winter solstice where the solar position is calculated and used in SMARTS to estimate the hourly solar irradiance data. The model Assumes a clear sky scenario due to the irregular variations of the local weather conditions which influence the solar irradiance, which allow us to consider the maximum possible solar irradiance.

B. System modelling

The photocurrent generated at the APD due to the optical power received from sunlight is given as:

$$I_{\rm b} = MA_{\rm d}\int_{350}^{750} P_{\rm D}^{\rm S}(\lambda)R(\lambda)T_{\rm bf}(\lambda)d\lambda, \tag{13}$$

where M is the gain of the APD, $A_{\rm d}$ is the APD detection area, $P_{\rm D}^{\rm S}(\lambda)$ is the direct sunlight irradiance given in W/m^2/nm, $R(\lambda)$ is the responsivity of the APD given in A/W, $T_{\rm bf}(\lambda)$ is the transmittance of the bandpass optical blue filter, and λ is the wavelength considered for the visible light spectrum mainly from 350 nm to 750 nm.

Similarly the photocurrent generated at the APD due to the optical power received from the m-LED is given as:

$$I_{\rm s} = MA_{\rm d}\int_{350}^{750} P_{\rm R}^{\rm L}(\lambda)R(\lambda)T_{\rm bf}(\lambda)d\lambda, \tag{14}$$

where $P_{\rm R}^{\rm L}(\lambda)$ is the received optical power of the m-LED given in W/m^2/nm, which was measured for 100 μm $\times$ 100 μm sized m-LED using a Labsphere spectral irradiance head (E1000).

The random arrival of incident photons results in shot noise which can be modelled by a Poisson distribution. However, when the number of incident photons increases, the shot noise is approximated by a Gaussian distribution. The shot noise variance is given by [20]:

$$\sigma_s^2 = 2qM^2F(I_b + I_s)B, \tag{15}$$

where q is the electron charge, B is the bandwidth of the APD, and F is the excess noise given as [21]:

$$F = \kappa M + (2 - 1/M)(1 - \kappa), \tag{16}$$

where κ is the holes/electrons ionization rate. The SNR at the receiver can be given by:

$$\text{SNR} = \frac{I_s^2}{\sigma_n^2}, \tag{17}$$

where $\sigma_n^2 = \sigma_s^2 + \sigma_t^2 + \sigma_d^2$ and σ_d^2 is the variance of the dark noise which is given as [20]:

$$\sigma_d^2 = 2qM^2FI_{dg}B + 2qI_{ds}, \tag{18}$$

where I_{ds} is the surface dark current and I_{dg} is the bulk dark current that experience the avalanche effect of the APD, and

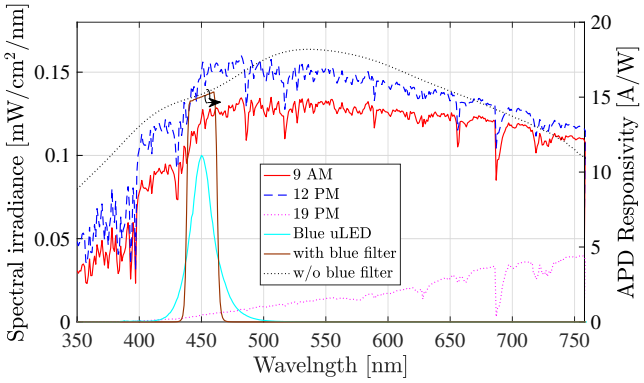

Fig. 2. The predicted sunlight irradiance in Antofagasta at 09:00, 12:00 and 19:00 on the 20th of December 2016 (left), alongside the spectral irradiance of the modelled m-LED centred at 450 nm, and response of the APD with and without considering the transmittance of the blue filter.

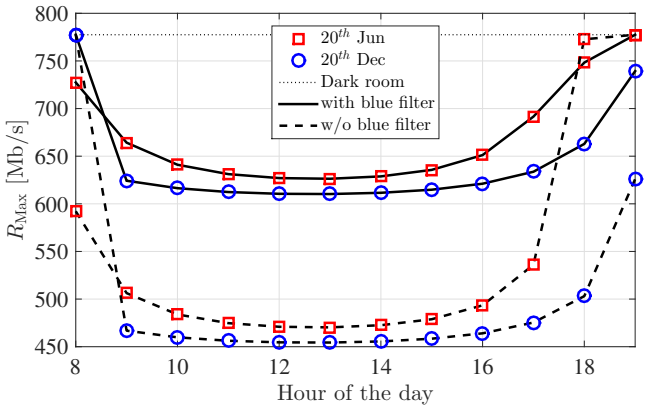

Fig. 3. Maximum achieved data rate given in Mb/s versus the time of the day on the 20th of December 2016 at Antofagasta for the three considered scenarios.

where $I_{\text{d}} = I_{ds} + MI_{dg}$. The variance of the thermal noise σ_T^2 is given by [22]:

$$\sigma_T^2 = 4\left(\frac{K_B T}{R_L}\right) F_n B, \tag{19}$$

where K_B is Boltzmann constant, T is the temperature in Kelvin, R_L is the load resistance given as 50 Ω, and F_n is the photodiode noise figure.

The maximum achievable data rate is calculated using the channel capacity limit defined by Shannon as [23]:

$$R_{\text{Max}} = B\log_2\left(1+\text{SNR}\right). \tag{20}$$

The system performance in terms of BER can be calculated using the the theoretical BER of real-valued M-QAM OFDM given for additive white Gaussian noise (AWGN) channels as [24]:

$$\text{BER}(M,\gamma) \cong \frac{4}{\log_2(M)}\left(1-\frac{1}{\sqrt{M}}\right)\times \sum_{l=1}^{R} \text{Q}\left((2l-1)\sqrt{\frac{3\log_2(M)\gamma}{2(M-1)}}\right), \tag{21}$$

where $Q(.)$ is the complementary cumulative distribution function (CCDF) for the standard normal distribution, γ is the SNR per bit, and $R = \min(2, \sqrt{M})$.

IV. Results and Discussions

The spectral irradiance of the modelled m-LED, and the responsivity of the modelled APD with and without considering the optical bandpass blue filter are shown in Fig. 2. In addition, the predicted spectral irradiance of the sunlight is shown at three different times of the summer solstice. It is shown that the solar irradiance is high at the ultra-violet (UV) and blue spectrum at sunrise. At sunset it becomes higher at the red and infra-red (IR) spectrum. The blue filter captures 70% of the m-LED irradiance.

The system performance is investigated for the summer and winter solstice as a function of the maximum achievable data rate versus the time of the day in Fig. 3. The performance of Scenario II (after blue filter) and the performance of Scenario III (w/o blue filter) are compared to the benchmark performance of Scenario I (dark room) when sunlight irradiance is not reaching the APD. It is shown that the data rate degrades by 41.6% at the noon of the winter solstice when the blue filter is not used. However, this degradation is reduced by more that 50% when the blue filter is introduced. Similar trends are shown for the summer solstice with less than 16 Mb/s difference compared to the winter solstice at noon.

The system performance as a function of the BER against the time of the day is shown in Fig.4(a) for 16-QAM OFDM. The results show the SNR degradation effect on the BER performance for the OFDM-based VLC system. Both scenario II and scenario III are shown to allow the use of forward error correction (FEC) in both winter and summer solstice, although a significant improvement is shown to be achieved when the blue filter is used. Similar trends are shown in Fig.4(b) for 64-QAM OFDM. However, the system performance of scenario II illustrate the significance of using the blue filter as FEC can not be used at BER$\geq 3.8\times10^{-3}$ [25].

Optical filtering is beneficial for other objectives in VLC. White illumination is generally achieved by coating the blue LED with a yellow phosphor which introduce a slow component into the frequency response of the LED. Blue filters are required to eliminate the slow response component of the yellow phosphor. Monochromatic light amplification by stimulated emission of radiations (LASERs) with narrowband optical filters in a wavelength division multiplexing (WDM)-based VLC system can guarantee a robust VLC system against sunlight irradiance with the potential of achieving data rates in the orders of Gb/s. On the contrary to the general belief that LiFi does not work under sunlight, sunlight is essential to solar cell based LiFi systems which can act as high speed LiFi receivers, while at the same time it can harvest energy from sunlight [26].

V. Conclusion

An outdoor VLC system is feasible in the presence of sunlight irradiance. Worst-case scenarios are considered in

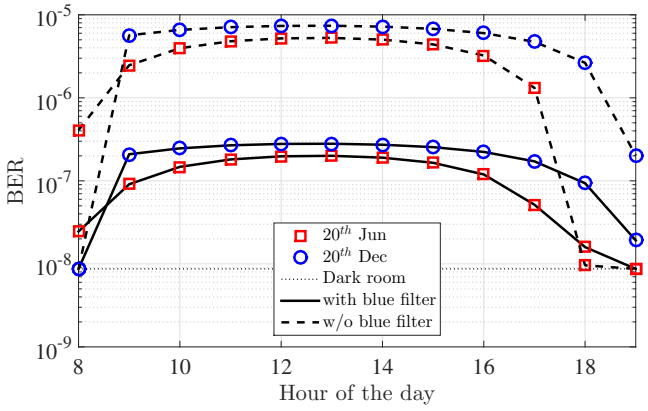

(a) 16-QAM OFDM

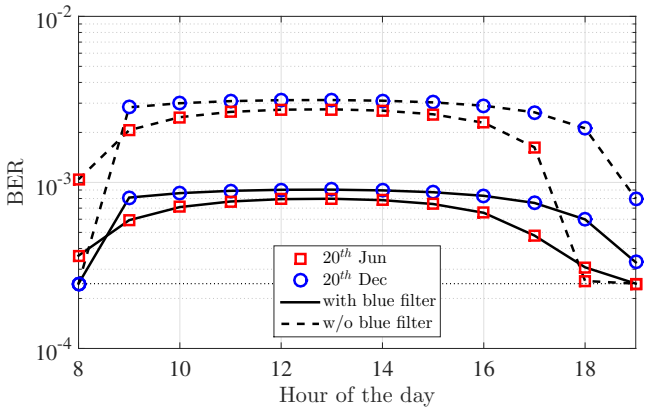

(b) 64-QAM OFDM

Fig. 4. BER of 64-QAM OFDM versus time of the day on the 20th of June 2016 at Antofagasta for the three considered scenarios.

this study to prove the concept of outdoor VLC systems. Shot noise caused by sunlight reduces the data rate of VLC systems. However, optical bandpass blue filters can limit the degradation caused by sunlight irradiance. An improvement of 50% can be achieved for the data rates using off-the-shelf blue filters. Data rates in the order of hundreds of Gb/s can be achieved in the presence of sunlight irradiance using LASERs with narrowband optical filters. Future work should consider the effect of automatic gain controller when saturation of the APD is considered.

Acknowledgment

This work was supported by the UK Engineering and Physical Sciences Research Council under Grants EP/K008757/1 and EP/M506515/1.

References

[1] Cisco Visual Networking Index, "Global Mobile Data Traffic Forecast Update, 2015-2020," CISCO, White Paper, Feb. 2016. [Online]. Available: http://www.cisco.com/c/en/us/solutions/collateral/service-provider/visual-networking-index-vni/mobile-white-paper-c11-520862.pdf

[2] OFCOM report, "Award of the 2.3 and 3.4 GHz Spectrum Bands: Competition Issues and Auction Regulations," OFCOM, Consultation , Jan. 2017. [Online]. Available: https://www.ofcom.org.uk/__data/assets/pdf_file/0026/93545/award-of-the-spectrum-bands-consultation.pdf

[3] S. Dimitrov and H. Haas, *Principles of LED Light Communications: Towards Networked Li-Fi*. Cambridge University Press, 2015.

[4] M. S. Islim, R. X. Ferreira, X. He, E. Xie, S. Videv, S. Viola, S. Watson, N. Bamiedakis, R. V. Penty, I. H. White, A. E. Kelly, E. Gu, H. Haas, and M. D. Dawson, "Towards 10 Gb/s Orthogonal Frequency Division Multiplexing-based Visible Light Communication Using a GaN Violet Micro-LED," *Photon. Res.*, vol. 5, no. 2, pp. A35–A43, Apr 2017. [Online]. Available: http://www.osapublishing.org/prj/abstract.cfm?URI=prj-5-2-A35

[5] D. Tsonev, S. Videv, and H. Haas, "Towards a 100 Gb/s Visible Light Wireless Access Network," *Opt. Express*, vol. 23, no. 2, pp. 1627–1637, Jan 2015. [Online]. Available: http://www.opticsexpress.org/abstract.cfm?URI=oe-23-2-1627

[6] G. Povey, "Top 10 Li-Fi Myths," June 2012. [Online]. Available: http://visiblelightcomm.com/top-10-li-fi-myths/

[7] M. S. Islim and H. Haas, "Modulation Techniques for Li-Fi," *ZTE Communications*, vol. 14, no. 2, pp. 29–40, April 2016.

[8] Y. H. Chung and S. B. Oh, "Efficient Optical Filtering for Outdoor Visible Light Communications in the Presence of Sunlight or Artificial Light," in *Intelligent Signal Processing and Communications Systems (ISPACS), 2013 International Symposium on*, Nov 2013, pp. 749–752.

[9] M. Beshr, C. Michie, and I. Andonovic, "Evaluation of Visible Light Communication system performance in the presence of sunlight irradiance," in *2015 17th International Conference on Transparent Optical Networks (ICTON)*, July 2015, pp. 1–4.

[10] T. Hamza, M.-A. Khalighi, S. Bourennane, P. Léon, and J. Opderbecke, "Investigation of Solar Noise Impact on the Performance of Underwater Wireless Optical Communication Links," *Opt. Express*, vol. 24, no. 22, pp. 25 832–25 845, Oct 2016. [Online]. Available: http://www.opticsexpress.org/abstract.cfm?URI=oe-24-22-25832

[11] ASTM, *Standard Solar Constant and Zero Air Mass Solar Spectral Irradiance Tables*, ASTM-E490-00a Std., 2014. [Online]. Available: https://doi.org/10.1520/E0490

[12] ——, *Standard Tables for Reference Solar Spectral Irradiances: Direct Normal and Hemispherical on 37 Tilted Surface*, ASTM G173-03 Std., 2014. [Online]. Available: https://doi.org/10.1520/G0173-03R12

[13] W. B. Stine and M. Geyer, *Power from the Sun*, 2001. [Online]. Available: http://Powerfromthesun.net

[14] A. Smets, K. Jäger, O. Isabella, M. Zeman, and R. van Swaaij, *Solar Energy: The Physics and Engineering of Photovoltaic Conversion, Technologies and Systems*. UIT Cambridge, 2016. [Online]. Available: https://books.google.co.uk/books?id=vTkdjgEACAAJ

[15] I. Reda and A. Andreas, "Solar Position Algorithm for Solar Radiation Applications," *Solar energy*, vol. 76, no. 5, pp. 577–589, 2004.

[16] C. A. Gueymard, "Parameterized Transmittance Model for Direct Beam and Circumsolar Spectral Irradiance," *Solar Energy*, vol. 71, no. 5, pp. 325–346, 2001.

[17] C. Gueymard, *SMARTS2: a Simple Model of the Atmospheric Radiative Transfer of Sunshine: Algorithms and Performance Assessment*. Florida Solar Energy Center Cocoa, FL, 1995.

[18] F. Xu, M. A. Khalighi, and S. Bourennane, "Impact of Different Noise Sources on the Performance of PIN- and APD-based FSO Receivers," in *Proceedings of the 11th International Conference on Telecommunications*, June 2011, pp. 211–218.

[19] R. Rondanelli, A. Molina, and M. Falvey, "The Atacama Surface Solar Maximum," *Bulletin of the American Meteorological Society*, vol. 96, no. 3, pp. 405–418, 2015. [Online]. Available: https://doi.org/10.1175/BAMS-D-13-00175.1

[20] Hamamatsu Photonics K.K, "Characteristics and Use of SI-APD (avalanche photodiode)," May 2004. [Online]. Available: http://neutron.physics.ucsb.edu/docs/Characteristics_and_use_of_SI_APD.pdf

[21] G. Keiser, *Optical Communications Essentials*. McGraw-Hill, 2003.

[22] J. M. Kahn and J. R. Barry, "Wireless Infrared Communications," *Proc. IEEE*, vol. 85, no. 2, pp. 265–298, Feb. 1997.

[23] C. Shannon, "A Mathematical Theory of Communication," *Bell System Technical Journal*, vol. 27, pp. 379–423 & 623–656, Jul. & Oct. 1948.

[24] F. Xiong, *Digital Modulation Techniques*, 2nd ed. Artech House Publishers, 2006.

[25] ITU-T, "Forward Error Correction for High Bit-rate DWDM Submarine Systems," ITU, Tech. Rep. ITU-T G.975.1, Retrieved Nov. 19, 2013 from http://www.itu.int/rec/T-REC-G.975.1-200402-I/en, 2004.

[26] Z. Wang, D. Tsonev, S. Videv, and H. Haas, "On the Design of a Solar-Panel Receiver for Optical Wireless Communications with Simultaneous Energy Harvesting," *IEEE J. Sel. Areas Commun.*, vol. 33, no. 8, pp. 1612–1623, Aug. 2015.